Thomson scattering in a low-pressure neon mercury positive column

Thomson scattering in a low-pressure neon mercury positive column

L. P. Bakker and G. M. W. Kroesen[a)]

Department of Applied Physics, Eindhoven University of Technology, P.O. Box 513, 5600 MB Eindhoven, The Netherlands

The electron density and the electron temperature in a low-pressure neon mercury positive column are determined using Thomson scattering. Special attention has been given to the stray light reduction in the Thomson scattering setup. The results are obtained in a discharge tube with a 26 mm diam, 10 mbar of neon, a mercury pressure inbetween 0.14 and 0.85 Pa, and an electric current ranging from 100 to 400 mA. The systematic error in the electron density is 15%–45%, the statistical error is 25%–35%. The total error in the electron temperature is 15%–35%. © *2001 American Institute of Physics.* [DOI: 10.1063/1.1390497]

I. INTRODUCTION

Radial cataphoresis is an interesting phenomenon in metal–vapor–noble-gas discharges. In the past, several authors report depletion of the metal atoms in these discharges.[1–5] When the metal atom density is sufficiently lowered by the radial cataphoresis process, noble gas excitation and ionization can take place. The transition from a metal vapor discharge (with the noble gas as a buffer gas) to the discharge in which both the metal vapor and the noble gas can be excited and ionized should be accompanied by an increase in the electron temperature. Experimental evidence of this increase is given by Van Tongeren.[3] He performed Langmuir probe measurements in sodium–noble-gas discharges. He measured the electron density and temperature over a large range of experimental conditions. He found a large increase in the electron temperature when the discharge current approached a critical value. At this critical current the noble gas was partly ionized. Cornelissen and Merks-Eppingbroek[4] used the mass balance for sodium to determine the electron density and temperature from the sodium density profile, which they obtained by laser absorption. They also performed Langmuir probe measurements under the same experimental conditions. The electron density derived from the probe measurements was a factor of 2.5 lower than the electron density obtained from the sodium atom density. This difference was attributed to the perturbation of the plasma by the Langmuir probe. This conclusion is important; a nonintrusive technique for the determination of the electron density and the electron temperature is needed. The best candidate for this determination is incoherent Thomson scattering.

Radial cataphoresis in mercury–neon discharges is attractive, since it can be used to control the discharge emission spectrum. In these mercury–neon discharges, we already investigated the onset of the excitation of neon atoms.[6] Furthermore, we measured the mercury ground state density profile[5] and the emission and excited state density profiles.[7]

With our Thomson scattering setup[8] we investigated the influence of radial cataphoresis on the electron velocity distribution function in an argon–mercury discharge.[9] Since these Thomson measurements are much easier to perform in such a discharge than in a neon–mercury discharge, this was our starting point. However, the explanation of the results of the measurements in mercury–neon discharges described above needs a better knowledge of the electron density and the electron temperature in such a discharge. Therefore, we also performed Thomson scattering measurements in a neon–mercury positive column. The main problem we had to solve in comparison with the measurements in the argon–mercury discharge is the very high intensity of the plasma emission in the Thomson scattering region. This article describes the electron density and temperature measurements we performed in a neon–mercury positive column under a number of different conditions. We are especially interested in the electron density and the electron temperature at a relatively low mercury pressure, where the emission of neon lines becomes significant.

II. EXPERIMENTAL SETUP

The Thomson scattering measurements have been performed with the setup described in Ref. 8. The setup consists of three parts. The first part consists of an excimer-pumped dye laser with an amplified spontaneous emission (ASE) filter. The second part consists of a lens focusing the laser beam in front of the detection branch, the discharge lamp, and a laser power monitor. The third part is the detection branch, which consists of a spectrograph with an Intensified charge coupled device (ICCD), two lenses making an image of the laser beam on the slit of a spectrograph, and a sodium vapor absorption cell. Figure 1 shows a schematic drawing of the setup. The first part of the setup produces a laser beam with a wavelength of 589.6 nm and a high spectral purity. This laser beam is shone through the discharge lamp and the scattered light is captured and subsequently guided through the sodium vapor absorption cell. This scattered light is then detected by the ICCD camera, which is mounted on the spectrograph. The slit of the spectrograph is positioned parallel to the laser beam, so the image of the laser beam is parallel

---

[a)]Author to whom correspondence should be addressed; electronic mail: g.m.w.kroesen@tue.nl
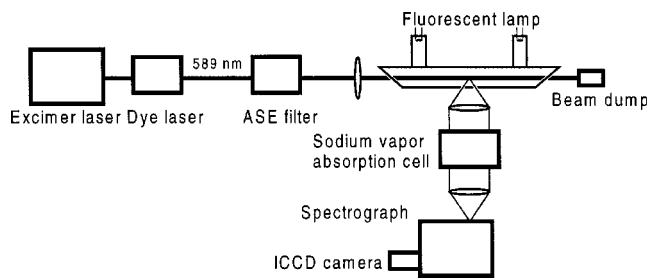
FIG. 1. The experimental setup for the Thomson scattering experiments.

with the slit. The Rayleigh scattering signal and the stray light are absorbed in the sodium cell, while the Thomson scattering photons are transmitted. In this way we obtain an efficient way of reducing the influence of stray light on the Thomson scattering spectrum.

With respect to the setup described in Ref. 8 we made some minor changes. In the detection branch, the two imaging lenses are replaced by lenses with a focal distance of 250 mm. The length of the slit is changed to 15 mm. The ICCD camera is covered partly, leaving the 590–594 nm region open. Furthermore, the discharge lamp itself is positioned in a box with a controllable temperature, and the mercury vapor pressure in the lamp is controlled using a thermostat bath. The lamp is a U-shaped borosilicate glass tube with Brewster windows at the ends. The inner diameter of the lamp is 23.2 mm, and its outer diameter is 26 mm. The neon pressure is 10 mbar. Just above the electrodes, two water jackets are positioned around the tube. With these jackets the tube is cooled locally. The temperature of these cold spots imposes the mercury vapor pressure in the tube. The water jackets are connected to a Haake thermostat bath. A schematic drawing of the discharge lamp is shown in Fig. 2. The discharge is sustained by a standard Philips BRC 411/01 35 kHz ballast.

The Thomson scattering setup is aligned by measuring the rotational Raman scattering spectrum in nitrogen. This spectrum is also used for the intensity calibration of the Thomson scattering measurements. The Raman scattering spectra are taken using a tube filled with 900 mbar of nitrogen. This tube is similar to the discharge tube. After the alignment of the setup is performed, the nitrogen tube is replaced by the discharge tube, leaving the rest of the setup unchanged. The laser power is measured with an Ophir AN/2 laser power monitor. The laser power used for the Thomson scattering spectra was approximately 1 W (time averaged) at a repetition rate of 150 Hz. We integrated the Thomson scattering spectrum for 60 min in order to improve the signal to noise
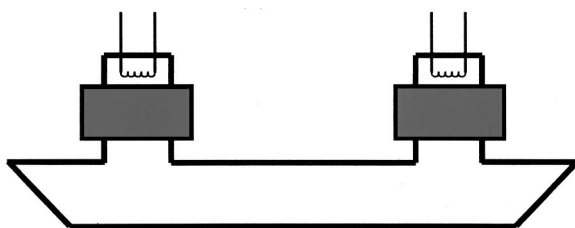

FIG. 2. Schematic drawing of the discharge lamp. The gray rectangles represent the water jackets.

ratio. The ICCD camera is used in the gated mode, where the gate width was 200 ns. The ICCD camera is read out in the full vertical binning mode. Besides this, along the horizontal (wavelength) axis the camera is read out per three pixels. The width of the response of the camera to a single photoelectron event is also three pixels. The discharge was stable enough to allow us to perform the plasma emission measurements after the Thomson scattering spectrum is obtained. This plasma emission is measured under the same experimental conditions as the Thomson scattering spectrum. The stray light spectrum is also obtained for every Thomson scattering measurement.

The net Thomson scattering spectrum is obtained by subtracting the plasma emission and the stray light from the raw Thomson scattering spectrum. The absolute intensity is obtained using the Raman scattering spectrum, which is measured before every Thomson scattering measurement. The Thomson scattering spectrum is then fitted using a Gaussian profile for the electron velocity distribution function. The fit is obtained using a least squares method. In the fitting procedure we only used the wings of the profile. From the fit, we obtain the electron density and the electron temperature.

The measurements are performed in five series. Series A is performed at a cold spot temperature of 18 °C. This temperature corresponds to a mercury vapor pressure of 0.14 Pa. The electrical current through the lamp was 100, 200, and 400 mA. In this series, the radial profiles of the electron density and the electron temperature are measured. Series B, C, D, and E are performed at the cold-spot temperatures of 18, 24, 30, and 40 °C, respectively. The corresponding mercury vapor pressures are 0.14, 0.24, 0.39, and 0.85 Pa. The dependency on the electrical current through the lamp is obtained between the currents of 100 and 400 mA. The electron density and the electron temperature are measured at the tube axis.

In a separate experiment, we measured the temperature of the outer tube wall at the position where the Thomson scattering spectra are measured. These temperature measurements are done for the conditions of series A, B, C, D, and E.

III. RESULTS

The measurements are performed as described in the preceding section. The ICCD camera had to be covered partly, suppressing the strong emission lines of neon. We used the spectral region inbetween the 588.2 and the 594.5 nm lines of neon. Only the wings of these lines could be detected. Assuming a Maxwellian energy distribution function, the distribution function of electrons with energies ranging from 0.5 to 5 eV could be measured. Although we suppressed the strongest lines in this way, there are ten weak neon lines remaining, overlapping the Thomson scattering spectrum. These weak lines resulted in an unexpected problem. The broadband ASE signal, which is suppressed by means of the ASE filter, can be absorbed by neon atoms in the lower state of the weak lines. This absorption is succeeded by emission. This additional emission is not present in the spectrum of the plasma without the laser. So when we subtract the plasma emission from the combined spectrum of
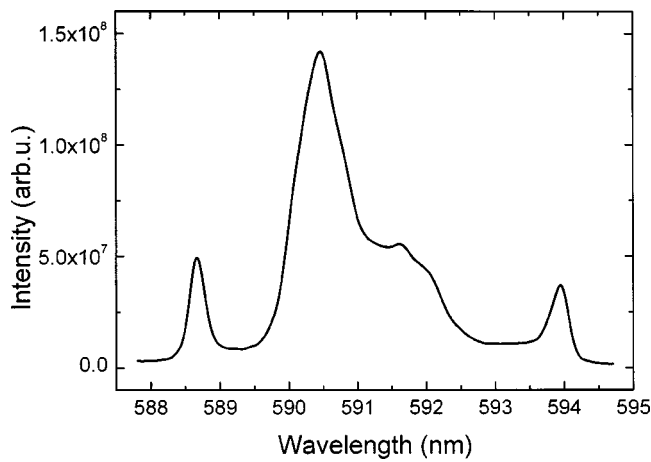
FIG. 3. The plasma emission for the cold-spot temperature of 18 °C, and a current of 400 mA.

FIG. 4. Example of a Thomson scattering spectrum, with the fitted profile.

the plasma and the laser, we obtain the Thomson scattering spectrum and some additional emission from the weak neon lines, which we will call laser induced fluorescence (LIF), for convenience. Normally, this additional emission can be detected in the spectrum by identifying the emission at a certain wavelength as a certain spectral line. This emission region can then be discarded in performing the fit of the Thomson scattering spectrum. In our case, however, the spectral profile of the additional emission is nearly equal to the spectral profile of the Thomson scattering signal, except for the 588.2 and the 594.5 nm lines, as can be seen in Fig. 3. This makes it very hard to discriminate between the Thomson scattering photons and the LIF photons. Based on the ASE level as measured in Ref. 8 and the density of the $2p$ states as given in Ref. 7, we can conclude that the LIF signal is of the same order of magnitude as the Thomson scattering signal for the measurements in series A and B. For series C, the LIF signal is much lower, and for series D and E, the LIF signal is negligible. We used the following method to approximate the correction for the LIF photons. The ratio of the LIF intensity to the intensity of the plasma emission for one spectral line is given by the following expression:

$$\frac{\Psi_{\mathrm{LIF}}}{\Psi_{\mathrm{plasma}}} = \frac{g_k}{g_i} \cdot \frac{n_i}{n_k} \cdot [1 - \exp(\tau_m/\tau_k)] \cdot a, \qquad (1)$$

where g_k and g_i are the statistical weights of the upper and the lower state, n_k and n_i are the densities of the upper and the lower state, τ_m is the gate width, τ_k is the lifetime of the upper state, and a is a constant depending on the geometry, the wavelength of the transition, and the ASE level of the laser.

The combined LIF and Thomson spectrum is now corrected by subtracting a fraction ξ of the plasma emission. The fraction ξ is chosen in such a way that the LIF signal of the 594.5 nm line vanishes. It can be shown using expression (1) that the ratio of the LIF intensity to the intensity of the plasma emission is the highest for this line. So this correction is too high for the weak neon lines. However for the fit, we only use the wavelength range where there is only the influence of two of the weak neon lines at approximately the
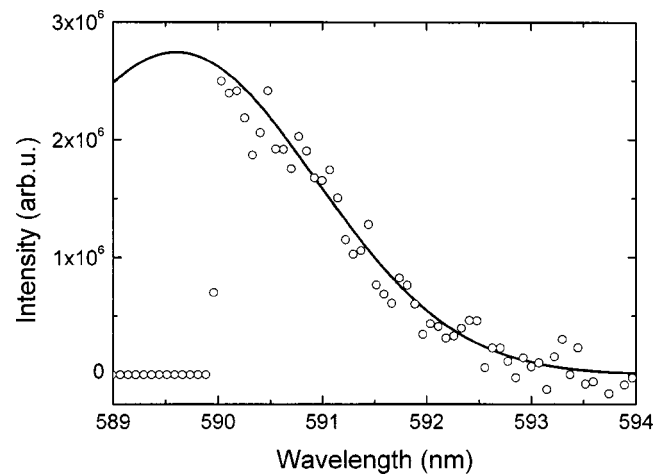
same wavelength (591.89 and 591.90 nm) and where the correction is less than 30% of the resulting Thomson scattering profile. This means that the measured electron density will be at maximum 30% too low. On the other hand, the spectral profile of the plasma emission in this region has a form similar to a Thomson scattering profile with the temperature of approximately 1.5 eV. Therefore, the influence of the LIF correction on the measured electron temperature is low, since the electron temperature of the plasma is also approximately 1.5 eV. This is also apparent in the correction for the LIF signal, which is approximately a constant fraction of the Thomson scattering spectrum over the region of interest for Thomson scattering.

An example of a measured Thomson scattering spectrum is shown in Fig. 4, along with a Gaussian fit of the data, representing the Maxwellian velocity distribution function. We fitted the measurements in series A, B, and C in the wavelength regions from 591.75 to 593.0 nm. This region corresponds to the energy range from 1.7 to 4.1 eV. The measurements in series D and E are fitted in the wavelength regions from 590.75 to 593.0 nm. This region corresponds to the energy range from 0.5 to 4.1 eV. A disadvantage of the fact that we only measure one side of the Thomson scattering spectrum is that the fitting procedure is less sensitive to the electron temperature. This is mainly caused by the fact that the width of the slit has been chosen larger than the image of the laser beam in the slit, in order to avoid artifacts by minor misalignment. This can lead to a slight error in the wavelength axis. This error is on the order of 0.07 nm. However, we checked the measurements where we covered part of the camera with Thomson measurements where we measured the whole spectrum under the same discharge conditions. This was only possible in the situation where the neon emission was low enough. Measuring the whole spectrum resulted in a difference of 4% in the electron density and 3% in the electron temperature. These differences are not significant, considering the experimental noise.

Figures 5(a) and 5(b) show the results of the measurements series A, the electron density, and the electron temperature as a function of the radial position r. In Fig. 4(a), the markers represent the measurements, and the drawn lines are
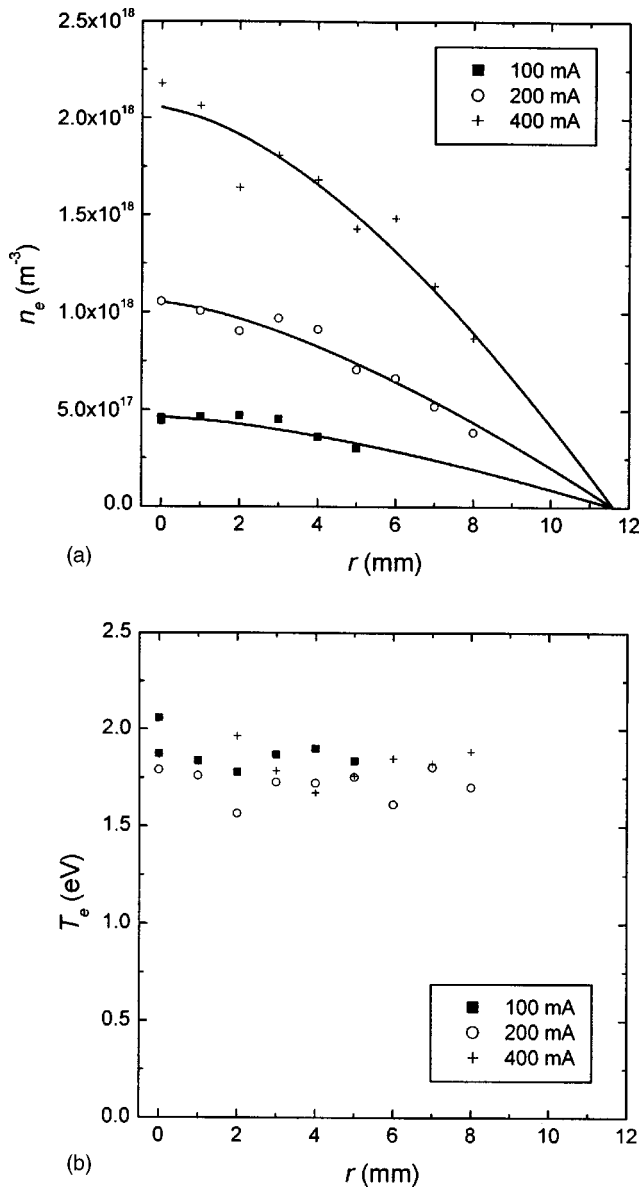
FIG. 5. (a) The electron density as a function of the radial position (series A). (b) The electron temperature as a function of the radial position.

FIG. 6. (a) The electron density as a function of the current (series B–E). (b) The electron temperature as a function of the current.

the fits of the measurements, using the following expression:

$$n_e(r) = n_{e0} \cdot [1 - (r/R)^m], \qquad (2)$$

where n_{e0}, and m are fitting parameters. This expression has been chosen for numerical convenience. Furthermore, its profiles are very similar to the commonly used Bessel profiles. It was not possible to measure the Thomson scattering profile closer to the tube wall, since the electron density was too low to have a reasonable amount of scattered photons. Figure 4(b) shows the electron temperature as a function of the radial position r. Considering the noise on the measurements, we cannot conclude that the electron temperature varies over the radius.

Figures 6(a) and 6(b) show the results of the measurement series B, C, D, and E, the electron density, and the electron temperature on the tube axis as a function of the electrical current. 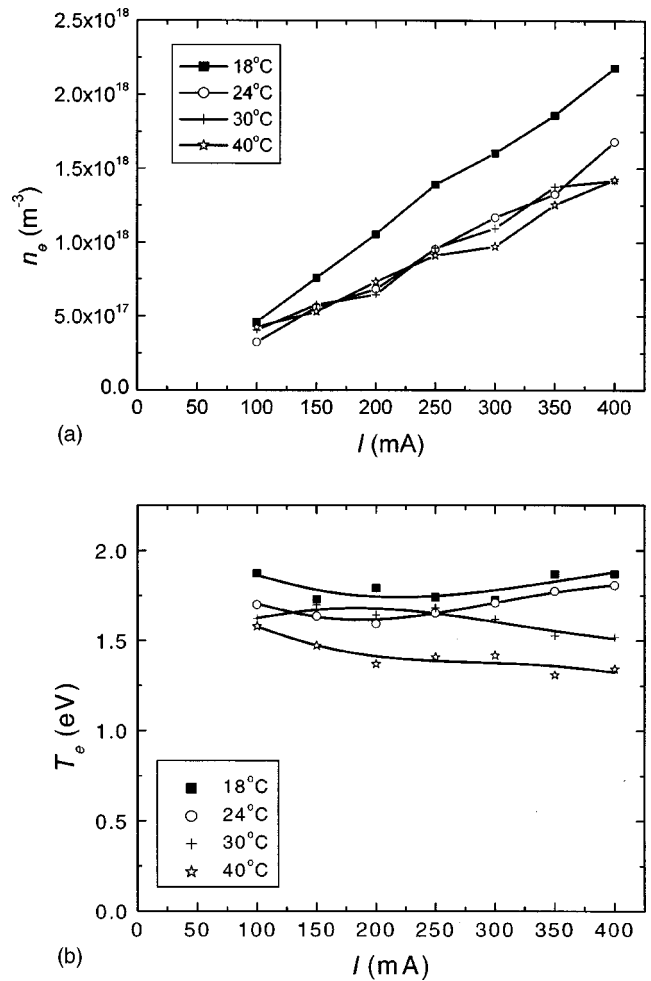It is clear that the electron density is a linear function of the current. This is in a first order approximation an effect of the increased power density in the discharge.

At the cold-spot temperature of 18 °C, the electron temperature does not significantly decrease or increase with the current. At 24 °C, the electron temperature first decreases, however, it increases at currents higher than 200 mA. At the other cold-spot temperatures, the electron temperature decreases with the current.

At the cold-spot temperature of 18 °C, neon excitation always occurs. For the temperature 24 °C, neon excitation is present at currents higher than 200 mA. This is clear in Fig. 7, where the emission of the weak neon lines is plotted as a function of the discharge current. Both regions where the emission of the weak neon lines is not zero correspond to a nondecreasing electron temperature in Fig. 5(b). For the higher cold-spot temperatures, neon excitation is absent, and the electron temperature decreases up to the current of 400 mA.

The trends in the electron temperature can be understood using the mass balance for electrons:

$$n_e n_{Hg} k_{Hg}(T_e) + n_e n_{Ne} k_{Ne}(T_e) = -\nabla[D_a(T_e) \cdot \nabla n_e], \quad (3)$$

where n_{Hg} is the mercury density, n_{Ne} is the neon density, k_{Hg}

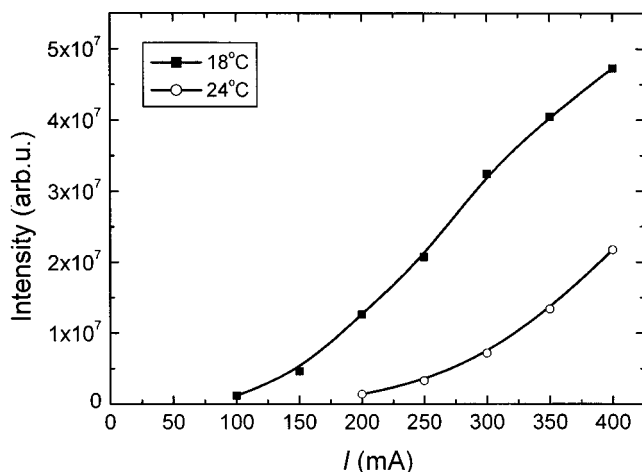FIG. 7. The emission of the weak lines of neon as a function of the current.

FIG. 8. The outer wall temperature of the tube for series A, B, and C–E.

is the ionization reaction coefficient for mercury, k_{Ne} is the ionization reaction coefficient for neon, and D_a is the ambipolar diffusion coefficient. Since the reaction coefficients are exponential functions of the electron temperature and the ambipolar diffusion coefficient is a linear function of this electron temperature, we can neglect the dependency of the right-hand side on the electron temperature. Furthermore, the ambipolar diffusion coefficient is determined mainly by the noble-gas pressure in the tube. As a first-order approximation, we can assume the ambipolar diffusion coefficient to be independent of the mercury pressure. Regarding the reaction coefficients we note that at higher electron densities, the electron temperature decreases due to the increase of multistep ionization contrast to direct ionization.

In general, the electron temperature is such that the ionization rate of mercury is much higher than the ionization rate of neon. So a change in the mercury density will have a large influence on the electron temperature, as can be concluded from the first term on the left-hand side of expression (3). When the mercury density is decreased, the electron temperature will increase since the decrease in the chance of an ionization collision has to be counterbalanced by increasing the chance of ionization during a collision, since the loss of charged particles is approximately constant. So the electron temperature decreases with increasing mercury pressure. This effect is clear in Fig. 5(b), where on the average, the electron temperature decreases with increasing mercury pressure.

A change in the current will be followed by a change in the electron density. This change in the electron density influences the electron temperature, by means of enhancing multistep or direct ionization. The change in the electron density also causes a change in the ambipolar flux to the wall, and subsequently a change in the mercury density, since the mercury density gradient is coupled to the gradient in the mercury ion density. The influence of this change in the mercury density is only significant in the situation with a low mercury pressure in the tube, i.e., at 18 and 24 °C. There, the ionization of neon can be significant, since the mercury ionization decreases with the mercury density. However, neon requires a higher electron temperature, since the excited
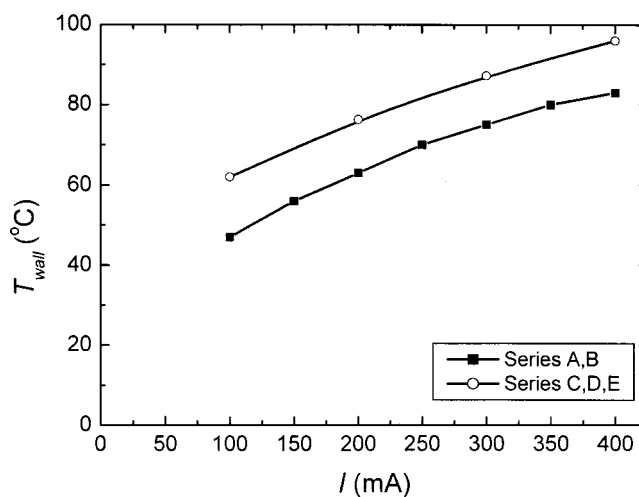
states possess a much larger energy than the corresponding states of mercury. The decrease of the electron temperature at low currents can be regarded as the increasing influence of multistep ionization. The behavior of the electron temperature at currents higher than 200 mA for the two lowest temperatures can be attributed to the increasing influence of neon ionization contrast to mercury ionization. This influence is absent at the two highest temperatures, since the mercury density and the mercury ionization rate remain high enough.

In the past, several authors report the necessity of taking into account the depletion of the high energetic tail of the electron energy distribution function in mercury–noble-gas discharges, see for instance Ref. 10. The loss of electron energy in inelastic collisions of electrons with mercury atoms in the ground state is not compensated by the energy gain in the reverse process. This is especially important for the $^3P_{0,1,2}$ triplet, which is mainly populated by collisions between ground state mercury and electrons and is mainly depopulated by resonant emission through the resonant state $^3P_1$. The depletion of the electrons with energies higher than 4.6 eV is more pronounced at low electron densities, since there is less Coulomb relaxation. We note that the electron temperature we measured is the temperature determined by the distribution function of electrons with energies lower than 4.1 eV, i.e., in the energy range in which we fit the data. In the investigation of the electron energy distribution function at the onset of neon excitation, the tail of the electron energy distribution function plays an important role. The tail electrons excite and ionize neon atoms. In the neon mercury positive column it is not possible to measure the tail electron distribution function using Thomson scattering due to the high level of plasma emission.

The outer wall temperature of the discharge tube at the position where the Thomson scattering spectra are obtained is plotted in Fig. 8, for series A, B, C, D, and E. Note that series A and B are measured without increasing the ambient temperature; these series are taken at an ambient temperature of 27 °C. The other series are taken at an ambient temperature of 50–56 °C.

IV. DISCUSSION

The accuracy in the measurements is limited by systematic and statistical errors. Systematic errors reduce the accuracy of the absolute value of the measured quantities, while the statistical errors reduce the reproducibility of the results. We will start with a discussion of the error in the electron density followed by an analysis of the error in the electron temperature.

A. Electron density

The absolute value of the electron density is dependent on the theoretical cross section used for rotational Raman scattering. The error in the absolute value of the electron density due to uncertainty in the calibration is approximately 15%.[9] For the measurements at the two lowest mercury pressures, there is an additional systematic error introduced by the correction for the LIF signal. For the 18 °C measurements, this additional error is at maximum 30%, for the 24 °C, this additional error is at maximum 10%.

In addition to the systematic error, we introduce a statistical error, i.e., noise in the experiment itself. The three most important sources of noise are the power monitor reading in the Raman and Thomson scattering experiments, the noise on the plasma emission, and the alignment of the setup. The statistical error in the electron density measurements adds up to roughly 25%. For the measurements at the lowest two mercury pressures, there is an additional statistical error caused by the fact that the region where the data could be fitted was smaller, resulting in a less accurate fit. This additional statistical error is approximately 10%.

B. Electron temperature

The systematic error in the absolute value of the electron temperature is very small. There are three possible components; instrumental broadening by the spectrograph, the calibration of the wavelength axis, and the fact that we only measure one side of the Thomson scattering spectrum. The influence of the apparatus profile is on the order of 1%. The wavelength axis could be calibrated very precisely, the resulting error is negligible. The influence of covering part of the ICCD camera is also very small, as can be concluded from a comparison between the measurements with and without covering the camera. For the measurements at the two lowest mercury pressures, there is an additional systematic error introduced by the correction for the LIF signal. For the 18 °C measurements, this additional error is at maximum 10%; for the 24 °C, this additional error is at maximum 5%.

The experimental noise in the electron temperature is caused by two factors. At first, the low amount of Thomson scattering photons results in a low signal to noise ratio per wavelength interval. Second, the noise on the plasma emission decreases the accuracy of the fit. The total error (systematic and statistical) in the electron temperature measurements is on the order of 15%–25%. For the measurements at the two lowest mercury pressures, there is an additional statistical error due to the fact that the wavelength region where the measurements can be fitted is smaller. A smaller region is used in order to limit the influence of the LIF correction. This additional error is approximately 10%.

As a concluding remark we note that the electron temperature we observe is the temperature of the electrons with an energy between 0.5 and 4.1 eV. In the corresponding velocity range the Thomson scattering spectrum can be fitted by a Maxwellian distribution function. The experimental noise was too high to make any comment on the question whether or not the electron velocity distribution function is non-Maxwellian outside this region.

[1] R. Bleekrode and J. W. van der Laarse, J. Appl. Phys. **40**, 2401 (1969).
[2] J. H. Waszink and J. Polman, J. Appl. Phys. **40**, 2403 (1969).
[3] H. F. J. van Tongeren, Philips Res. Rep., Suppl. **3**, 35 (1975).
[4] H. J. Cornelissen and H. J. H. Merks-Eppingbroek, J. Appl. Phys. **59**, 2324 (1986).
[5] L. P. Bakker and G. M. W. Kroesen, Appl. Phys. Lett. **76**, 1528 (2000).
[6] L. P. Bakker, P. van den Oever, and G. M. W. Kroesen, Plasma Sources Sci. Technol. **7**, 600 (2000).
[7] L. P. Bakker and G. M. W. Kroesen, J. Appl. Phys. **88**, 1733 (2000).
[8] L. P. Bakker, J. M. Freriks, F. J. de Hoog, and G. M. W. Kroesen, Rev. Sci. Instrum. **71**, 2007 (2000).
[9] L. P. Bakker and G. M. W. Kroesen, J. Appl. Phys. **88**, 3899 (2000).
[10] K. Wani, J. Appl. Phys. **67**, 6130 (1990).